

Convergent Iterative Closest-Point Algorithm to Accomodate Anisotropic and Inhomogenous Localization Error

Lena Maier-Hein, Alfred M. Franz, Thiago R. dos Santos, Mirko Schmidt, Markus Fangerau, Hans-Peter Meinzer, and J. Michael Fitzpatrick, *Fellow, IEEE*

Abstract—Since its introduction in the early 1990s, the Iterative Closest Point (ICP) algorithm has become one of the most well-known methods for geometric alignment of 3D models. Given two roughly aligned shapes represented by two point sets, the algorithm iteratively establishes point correspondences given the current alignment of the data and computes a rigid transformation accordingly. From a statistical point of view, however, it implicitly assumes that the points are observed with isotropic Gaussian noise. In this paper, we show that this assumption may lead to errors and generalize the ICP such that it can account for anisotropic and inhomogenous localization errors. We 1) provide a formal description of the algorithm, 2) extend it to registration of *partially overlapping* surfaces, 3) prove its convergence, 4) derive the required covariance matrices for a set of selected applications, and 5) present means for optimizing the runtime. An evaluation on publicly available surface meshes as well as on a set of meshes extracted from medical imaging data shows a dramatic increase in accuracy compared to the original ICP, especially in the case of partial surface registration. As point-based surface registration is a central component in various applications, the potential impact of the proposed method is high.

Index Terms—Registration, surface algorithms, ICP, point-based registration, anisotropic weighting.

1 INTRODUCTION

REGISTERING 3D models is an important task in a variety of fields, including biometrics [1], 3D model construction from multiple range images [2], intra-interventional registration in computer-assisted medical applications [3], and quality assurance in manufacturing [4]. While many different methods have been proposed for finding a rough alignment of the data [5], the Iterative Closest Point (ICP) algorithm [6] is probably the most widely used method for *fine* geometric alignment of 3D models. The general idea behind it was introduced in the early 1990s almost simultaneously by several authors [6], [7], but the variant proposed by Besl and McKay [6] is the most frequently cited one. It is generically applicable to any two objects represented by point clouds and can be proven to converge to an at least local minimum with respect to a mean-square distance metric. Given two roughly aligned shapes represented by two point sets, the algorithm iteratively 1) establishes point correspondences

given the current alignment of the data, and 2) computes a rigid transformation accordingly. From a statistical point of view, however, it implicitly assumes that the points are observed with zero mean, identical, and isotropic Gaussian noise. In the context of surface registration, this implies that corresponding points should correspond to the same physical location, as illustrated in Fig. 1. This will, however, generally not be the case, e.g., because of differences in mesh resolution. Furthermore, point localization errors may be highly anisotropic. Laser range scanners or Time-of-Flight (ToF) cameras [8], for instance, typically have a much higher localization uncertainty in the viewing direction of the camera, which may lead to errors when establishing point correspondences, as shown in Fig. 2a.

Although various ICP variants have been proposed in the literature (cf., Section 2), the issue of anisotropic localization errors has so far been given very little attention. This may be due to the fact that all known closed-form solutions for registering two point sets with known correspondences implicitly assume isotropic noise, as stated by Balachandran and Fitzpatrick [9]. The closest work to ours was proposed by Estépar et al. [10], who proposed a variant of the ICP that incorporates covariance matrices for all points to be registered upon finding the optimal rigid transformation for a set of corresponding points. It is based on a method proposed by Ohta and Kanatani [11] for optimal rotation estimation from two sets of points in the presence of anisotropic inhomogenous noise. However, the standard closest point operator based on the euclidean distance is applied for establishing the point correspondences. As a consequence of this, an *increase* of the corresponding cost function may occur, and the algorithm is not guaranteed to terminate.

- L. Maier-Hein, A.M. Franz, T.R. dos Santos, M. Fangerau, and H.-P. Meinzer are with the Division of Medical and Biological Informatics, German Cancer Research Center (DKFZ), Neuenheimer Feld 280, Heidelberg D-69120, Germany. E-mail: l.maier-hein@dkfz-heidelberg.de.
- M. Schmidt is with the Heidelberg Collaboratory for Image Processing, Digital Image Processing Group, University of Heidelberg, Speyerer Str. 6, Heidelberg 69115, Germany.
- J.M. Fitzpatrick is with the Department of Electrical Engineering and Computer Science, Vanderbilt University, 2301 Vanderbilt Place, Nashville, TN 37235-1679.

Manuscript received 29 Mar. 2011; revised 22 Aug. 2011; accepted 6 Nov. 2011; published online 13 Dec. 2011.

Recommended for acceptance by I. Reid.

For information on obtaining reprints of this article, please send e-mail to: tpami@computer.org, and reference IEEECS Log Number TPAMI-2011-03-0184.

Digital Object Identifier no. 10.1109/TPAMI.2011.248.

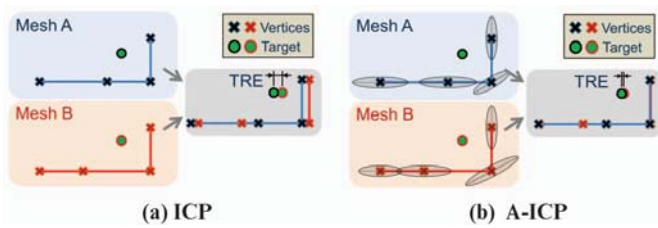


Fig. 1. Schematic illustration of the computation of a rigid transformation based on a set of corresponding points in meshes A and B with (a) the original ICP and (b) the proposed A-ICP. For a better illustration, a 2D representation was chosen. In (a), a considerable misregistration occurs because two of the corresponding vertices (central vertices) do not correspond to the same physical position. In (b), we compensate for this effect by setting the point localization accuracy based on the area of influence of a vertex (represented by the dimensions of the ellipsoids drawn in that direction), which leads to a decrease in the TRE.

In this paper, we present the first variant of the ICP that accounts for anisotropic localization uncertainty in *both* input point sets as well as in *both* steps of the algorithm and prove that the associated cost function decreases in every iteration. The localization error associated with a point is integrated into the algorithm via a covariance matrix representing a zero-mean Gaussian distribution. Depending on the application, the latter can be defined by the user or derived directly from the data. We will refer to this generalized ICP variant as anisotropic ICP (A-ICP).

A preliminary version of this work was presented at the SPIE Medical Imaging Symposium [12]. However, the paper has been extended significantly, and all experiments are new. Major extensions include:

1. A detailed description of the A-ICP algorithm including a method for making its fiducial registration error (FRE) comparable to the FRE of the ICP by Besl and McKay [6].
2. A derivation of the required covariance matrices for a set of selected applications.
3. A variant of the algorithm for registration of *partially overlapping* surfaces.
4. Means for runtime optimization.
5. New experiments with (partially) publicly available data sets.

The remaining part of this paper is structured as follows: Section 2 gives an overview of the ICP variants published so far. Section 3 describes our algorithm in detail, including a variant that can be applied to partially overlapping surfaces. As a reasonable choice of covariance matrices is crucial to the performance of the algorithm, Section 4 presents two representative detailed examples for deriving covariance matrices for selected applications. Finally, Section 5 describes the experiments we performed to assess the performance of our algorithm, while Section 6 concludes with a discussion of this paper in the context of related work.

2 RELATED WORK

According to Rusinkiewicz and Levoy [13], the ICP algorithm was introduced in parallel work by Besl and McKay [6] and Chen and Medioni [7]. While Chen and Medioni [7] considered the more specific problem of

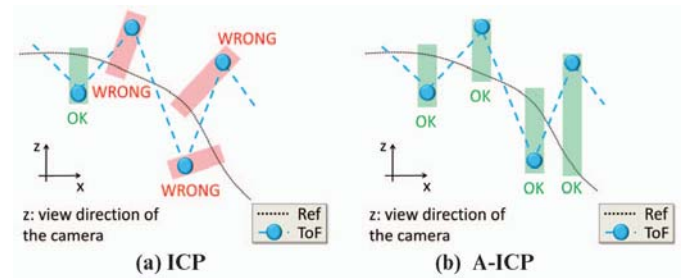


Fig. 2. (a) Schematic illustration of the establishment of point correspondences with (a) the original ICP and (b) the A-ICP. Reference mesh (represented by black dotted line), sparse noisy mesh (represented by connected vertices), and correspondences (boxes) are shown for the standard closest point operator based on the euclidean distance and the new closest point operator with less weight given to the direction z .

aligning range data, the paper by Besl and McKay [6] directly addresses the registration of 3D shapes represented by point clouds and is the most frequently cited ICP paper. The described algorithm has the important property of being provably convergent with respect to a least-square distance metric and is typically regarded as the reference/original/basis/standard ICP algorithm. In a review paper, Rusinkiewicz and Levoy [13] classified the proposed variants of the algorithm as affecting one of the six subtasks:

1. *Selection* (i.e., choosing subsets of X and Y).
2. *Matching*.
3. *Weighting* (correspondences).
4. *Outlier removal*.
5. *Error metric*.
6. *Minimization* (of the error).

Below, we provide a brief review of the proposed variants, focusing on those stages that we modified, namely, matching, error metric, and minimization.

2.1 Selection

Choosing subsets of the input point sets provided is usually performed with the purpose of speeding up the algorithm and/or removing outliers. Methods proposed in this context include uniform subsampling [14], random subsampling [15], selection based on intensity or color information [16], and selection of points such that the distribution of normals is as large as possible (*normal-space sampling*) [13].

2.2 Matching Points

In the original ICP algorithm by Besl and McKay [6], the euclidean distance was used as the distance metric for establishing point correspondences. Since then, a lot of variants have been proposed which include additional properties such as color [17], invariant features [18], [19], or surface normals [20] in the distance metric. The application of fuzzy correspondences was investigated repeatedly, among others in an expectation maximization (EM) variant of the ICP introduced by Granger et al. [21]. A technique referred to as *normal shooting* [7] determines the corresponding point to a point \vec{p} on a range image's surface by finding the intersection of the reference surface with the ray defined by \vec{p} and $\vec{n}_{\vec{p}}$, where $\vec{n}_{\vec{p}}$ is the normal vector in \vec{p} , thus

addressing the problem illustrated in Fig. 2a. For the same purpose, Kaneko et al. [22] proposed an M-estimation-based method for establishing correspondences, which allows for assigning different weights to different coordinate axes. Furthermore, a method called *reverse calibration* [23], [24] has been proposed: A given point on the mesh corresponding to the range image is projected onto the reference mesh from the point of view of the range camera. Other authors have introduced point-to-ray [25] or point-to-plane [2] metrics for addressing the same issue. Finally, Hansen et al. [26] applied the Mahalanobis distance [27] to allow for assigning anisotropic noise to the reference surface. One general problem associated with this and most other methods is the fact that they alter the convergence properties of the algorithm. Furthermore, none of the proposed methods allows incorporation of the covariance matrices of all input points into the correspondence computation.

2.3 Weighting

Several authors have also investigated assigning weights to point pairs in order to improve the robustness of the algorithm. The proposed methods range from assigning weights based on the interpoint distance [17], the compatibility of normals [13], or colors [17] or weighting based on the noise characteristics of a range camera [13]. However, the weighting is generally performed using scalar values or along certain directions of a common coordinate system [22], and none of the proposed methods incorporate covariance matrices in order to perform anisotropic, inhomogeneous weighting.

2.4 Outliers

As outliers have a large effect on methods based on least squares minimization, several methods have been proposed to detect and reject pairs that could have a negative effect on the registration result. Among others, rejection of the worst ξ percent [20], [28] pairs, rejection of pairs with a distance above a certain threshold [13], rejection of pairs on mesh boundaries [14], and rejection of pairs that are not consistent with neighboring pairs [25] have been proposed.

2.5 Error Metric and Minimization

In most algorithms, the sum of squared distances between corresponding points is minimized using one of the closed form solutions for determining the rigid transformation that minimizes this error (e.g., [29]). Alternatively, point-to-point metrics incorporating color [30] or point-to-plane metrics [7] were proposed. While closed form solutions for determining the rigid transformation that minimizes the mean-squared distance between corresponding points (e.g., [29]) exist, *iterative* optimization strategies must be applied for other error metrics such as the point-to-plane metric [7]. Several strategies have been proposed to improve robustness of the algorithm, including stochastic search using simulated annealing [7], [23], multiresolution strategies [31], using various randomly selected subsets in each step and choosing the optimum [15], and perturbing the points [32], [33] to prevent the algorithm from converging to only a local minimum. As already mentioned above, Estépar et al. [10] proposed a variant of the ICP algorithm that minimizes an FRE that accounts for anisotropic noise in the input data.

As the standard closest point operator based on the euclidean distance is applied, however, convergence of the algorithm cannot be guaranteed.

2.6 Further Variants

One of the main drawbacks of the ICP is its quadratic complexity $O(N^2)$ with the number of points N . Hence, various methods have been proposed for accelerating the algorithm by using *kd*-trees [32], closest point caching [32], a graphics processing unit (GPU) implementation [34], or parallelization on the central processing unit (CPU) [35], for example, when determining nearest neighbors. Other variants have investigated the incorporation of prior knowledge [36] and extending the ICP for nonrigid surface registration [18], [36], [37], [38], [39].

In conclusion, although some of the proposed variants address the issues associated with anisotropic localization errors to some extent, they are generally restricted to only a certain type/direction of uncertainty. To our knowledge, no method has been proposed so far that generalizes the original ICP such that prior knowledge can be integrated in a flexible manner and convergence can still be guaranteed.

3 ANISOTROPIC ICP (A-ICP)

In general, the goal of the original ICP [6] algorithm is to find a rigid transformation that registers two shapes that can be represented by two point sets $X = \{\vec{x}_1, \dots, \vec{x}_{N_X}\}$ and $Y = \{\vec{y}_1, \dots, \vec{y}_{N_Y}\}$. In the case of the original ICP, each iteration consists of two basic steps:

1. *Establishing correspondences*: For each $\vec{x}_i \in X$ a corresponding point $\vec{z}_i = C(\vec{x}_i, Y) \in Y$ is determined based on the euclidean distance $C(\vec{x}_i, Y) = \arg \min_{\vec{y}_j \in Y} \|\vec{x}_i - \vec{y}_j\|$.
2. *Computing the transformation*: Based on the established correspondences, a rigid transformation represented by a rotation matrix R and a translation vector \vec{t} is determined which minimizes the FRE, defined as root-mean-square (RMS) distance between corresponding points:

$$FRE_{std}^2 = \sum_{i=1}^N \|(R\vec{x}_i + \vec{t} - \vec{z}_i)\|_2^2. \quad (1)$$

The established transformation is then applied to the moving point set X .

The fact that both steps of the algorithm lead to a decrease in the FRE ensures convergence of the algorithm (cf., Appendix A, which can be found in the Computer Society Digital Library at <http://doi.ieeecomputersociety.org/10.1109/TPAMI.2011.248>). As already mentioned above, this procedure implicitly assumes that the input point sets are subject to isotropic zero-mean Gaussian noise. In this paper, we generalize the algorithm such that it can cope with anisotropic localization errors. For this purpose, we assume that the localization error in each point $\vec{p} \in X \cup Y$ is normally distributed with zero-mean and a covariance matrix $\Sigma_{\vec{p}} = V_{\vec{p}} S_{\vec{p}}^2 V_{\vec{p}}'$, where the columns of $V_{\vec{p}}$ are the principal axes of the localization error and $S_{\vec{p}} = \text{diag}(\sigma_{\vec{p},1}, \sigma_{\vec{p},2}, \sigma_{\vec{p},3})$ is a diagonal matrix with $\sigma_{\vec{p},j}$ representing the standard deviation

along the principal axis j . Note that $V_{\bar{p}}'$ denotes the transposed matrix of $V_{\bar{p}}$. In the following sections, we show how to incorporate these covariance matrices into both steps of the iterative algorithm (cf., Sections 3.1 and 3.2). We derive a formal description of the A-ICP (Section 3.4) and normalize the weighted FRE such that it compares to the FRE of the original ICP in the case of isotropic homogenous noise (Section 3.4). Finally, we introduce a variant of the A-ICP for registration of partially overlapping surfaces (Section 3.5) and present means for runtime optimization of the algorithm (Section 3.6).

3.1 Closest Point Operator

To determine the anisotropically weighted distance between two points \vec{x} and \vec{y} whose localization errors are assumed to be independent and represented by the covariance matrices $\Sigma_{\vec{x}}$ and $\Sigma_{\vec{y}}$, respectively, we determine the two-space cross covariance of the localization error as $\Sigma_{\vec{x}\vec{y}} = \Sigma_{\vec{x}} + \Sigma_{\vec{y}}$ (cf., [40]). The anisotropically weighted distance between \vec{x} and \vec{y} can then be defined as the weighted euclidean distance

$$d_{new}(\vec{x}, \vec{y}) = \|W_{\vec{x}\vec{y}}(\vec{x} - \vec{y})\|_2, \quad (2)$$

with the weighting matrix $W_{\vec{x}\vec{y}} = w\Sigma_{\vec{x}\vec{y}}^{-\frac{1}{2}}$ and a normalization constant $w > 0$, which can be used for normalization of the weighted FRE, as shown in Section 3.4. Note that $d_{new}(\vec{x}, \vec{y})$ represents the Mahalanobis distance [27] between \vec{x} and \vec{y} for the case that \vec{x} and \vec{y} are assumed to originate from a common multivariate Gaussian distribution with covariance matrix $\frac{1}{w^2}\Sigma_{\vec{x}\vec{y}}$: $d_{new}(\vec{x}, \vec{y})^2 = (\vec{x} - \vec{y})' w^2 (\Sigma_{\vec{x}\vec{y}})^{-1} (\vec{x} - \vec{y})$. Based on the weighted distance, we compute the closest point $\vec{y} = C_{new}(\vec{x}, Y)$ in a set of points Y to a given point \vec{x} as

$$C_{new}(\vec{x}, Y) = \arg \min_{\vec{y}_i \in Y} d_{new}(\vec{x}, \vec{y}_i). \quad (3)$$

Note that in the case of zero mean, identical, isotropic noise, we obtain covariance matrices $\Sigma_{\vec{y}} = \Sigma_{\vec{x}} = cI$ for some scalar value c and hence a weighting matrix $W_{\vec{x}\vec{y}} = W = \frac{w}{\sqrt{2c}}I$ for all points \vec{x}, \vec{y} , with I denoting the identity matrix. As a consequence, the new closest point operator yields the same result as the standard closest point operator $C(\vec{x}, Y) = \arg \min_{\vec{y}_i \in Y} \|(\vec{x} - \vec{y}_i)\|_2$.

3.2 Weighted Corresponding Point Registration

Each iteration of the generic ICP algorithm requires computation of an optimal rigid registration based on a set of corresponding points $(\vec{x}_i, \vec{z}_i); i = 1 \dots N_X$, where \vec{z}_i represents a point in Y .¹ We apply an extension of a recently published algorithm [9], [40] for registering the two point sets X and $Z = \{\vec{z}_1, \dots, \vec{z}_{N_X}\}$. The method assumes that the principal components of the localization error in each point are independent and normally distributed with zero means for both shapes, and it requires the associated covariance matrices $\Sigma_{\vec{x}_i}$ and $\Sigma_{\vec{z}_i}$ as input. The method iteratively minimizes the anisotropically weighted fiducial registration error ($FRE_{weighted}$):

1. Note that we introduced the set Z to facilitate dealing with indices. It contains the same number of points as X and has the property that \vec{x}_i corresponds to \vec{z}_i .

$$FRE_{weighted}^2 = \sum_{i=1}^N \|W_i(R\vec{x}_i + \vec{t} - \vec{z}_i)\|_2^2, \quad (4)$$

where W_i is a function of the rotation matrix R , $W_i = w(R\Sigma_{\vec{x}_i}R' + \Sigma_{\vec{z}_i})^{-\frac{1}{2}}$, and w is a normalization constant. For this purpose, the rigid transformation is initialized by solving 4 for isotropic, homogenous noise (i.e., with all W_i set to I). The strategy of the algorithm is then to replace, at each iterative step, the exact, nonlinear problem of minimizing (4) with a simple, linear problem, which can be solved exactly by linear algebra. Details can be found in [9] and [40]. For this paper, we modified the algorithm such that the solution to the isotropic registration problem is only used as the initial estimate if it returns a better $FRE_{weighted}$ than the identity transformation. Furthermore, if $FRE_{weighted}$ increases in an iteration, the previous transformation is returned. This case will generally not occur, but the modification is necessary in order to *guarantee* convergence of the A-ICP, as shown in Appendix A, available in the online supplemental material.

3.3 Algorithm

Given the covariance matrices $\Sigma_{\bar{p}}$ for each point $\bar{p} \in X \cup Y$, the aim of the A-ICP algorithm is to find a rotation matrix R and a translation vector \vec{t} such that the following error metric is minimized:

$$FRE_{weighted}^2(R, \vec{t}) = \sum_{i=1}^{N_X} \|W_i(R\vec{x}_i + \vec{t} - \vec{y}_{idx(i)})\|_2^2, \quad (5)$$

where $idx(i)$ is the index of the point $\vec{y}_{idx(i)} = C_{new}(R\vec{x}_i + \vec{t}, Y)$ in Y and $W_i = w(R\Sigma_{\vec{x}_i}R' + \Sigma_{\vec{y}_{idx(i)}})^{-\frac{1}{2}}$. This is achieved by iteratively 1) establishing point correspondences with the new closest point operator C_{new} given the current alignment of the data, and 2) computing a rigid transformation for mapping the current corresponding points using the modified corresponding point registration algorithm (cf., Section 3.2). In each iteration, the rigid transformation established is applied to transform the moving point set X and to propagate the associated covariance matrices.

The details are as follows:

1. Initialize variables: $k = 1$; $X^1 = X$; $FRE_{weighted}^0 = \infty$; $R^0 = I$; $\vec{t}^0 = \vec{0}$; $\Sigma_{\vec{x}_i}^0 = \Sigma_{\vec{x}_i}$; $i = 1, \dots, N_X$.
2. Compute the current corresponding points $Z^k = \{\vec{z}_i^k\}$, $i = 1, \dots, N_X$, with $\vec{z}_i^k \in Y$ being the closest point to $\vec{x}_i \in X^k$ according to the new distance measure:

$$idx(i)^k = \arg \min_j d_{new}(\vec{x}_i^k, \vec{y}_j), \quad (6)$$

$$\vec{z}_i^k = \vec{y}_{idx(i)^k}. \quad (7)$$

For this purpose, compute the current covariance matrix $\Sigma_{\vec{x}_i}^k$, the current cross-covariance matrix $\Sigma_{i,j}^k$, the current weighting matrix $W_{i,j}^{k-1}$, and the current distance $d_{new}(\vec{x}_i^k, \vec{y}_j)$ for each transformed point $\vec{x}_i^k \in X^k$ and each $\vec{y}_j \in Y$ as follows:

$$\Sigma_{\vec{x}_i}^k = R^{k-1} \Sigma_{\vec{x}_i}^{k-1} (R^{k-1})', \quad (8)$$

$$\Sigma_{ij}^k = \Sigma_{\vec{x}_i}^k + \Sigma_{\vec{y}_j}, \quad (9)$$

$$W_{ij}^{k-1} = w(\Sigma_{ij}^k)^{-\frac{1}{2}}, \quad (10)$$

$$d_{new}(\vec{x}_i^k, \vec{y}_j) = W_{ij}^{k-1}(\vec{x}_i^k - \vec{y}_j). \quad (11)$$

3. Compute the rotation matrix R^k , the translation vector \vec{t}^k , and the registration error $FRE_{weighted}^k$ for mapping the point set X^k onto the point set Z^k using the weighted point registration algorithm described above with the covariance matrices $\Sigma_{\vec{z}_i}^k = \Sigma_{\vec{y}_{idx(i)^k}}$ and $\Sigma_{\vec{x}_i}^k$

$$(R^k, \vec{t}^k) = \arg \min_{R, \vec{t}} \sum_{i=1}^{N_X} \|W_i^k (R\vec{x}_i^k + \vec{t} - \vec{z}_i)\|_2^2, \quad (12)$$

$$FRE_{weighted,k} = \sqrt{\sum_{i=1}^{N_X} \|W_i^k (R^k \vec{x}_i^k + \vec{t}^k - \vec{z}_i^k)\|_2^2}, \quad (13)$$

where W_i^k is computed automatically by the algorithm

$$W_i^k = w(R^k \Sigma_{\vec{x}_i}^k (R^k)' + \Sigma_{\vec{z}_i}^k)^{-\frac{1}{2}}. \quad (14)$$

4. Apply the rigid body transformation computed in the previous step to X^k to obtain the transformed point set X^{k+1} for the next iteration $k+1$: $x_i^{k+1} = R^k x_i^k + \vec{t}^k$.
5. If $|FRE_{weighted,k} - FRE_{weighted,k-1}| < \epsilon$ or the maximum number of iterations has been reached, terminate. Otherwise, set $k := k+1$ and go to step 2.

It can be seen that if the covariance matrices are set to the identity matrix I for all points, and w is set to $w = \sqrt{\frac{2}{N_X}}$ the weighted FRE ($FRE_{weighted}$) (cf., 13) is identical to the RMS distance between corresponding points and thus to the FRE of the original ICP. Hence, the original formulation of the ICP is obtained. As an important property, the A-ICP can be guaranteed to terminate after a finite number of iterations, as shown in Appendix A, available in the online supplemental material.

3.4 Normalization of FRE

Generally, the size of $FRE_{weighted}$ is somewhat arbitrary, as already stated in [40]. In fact, it decreases with increasing variances of the points. For example, if we set all covariance matrices to $\Sigma = s^2 I$, we obtain the same weighting matrix $W = w(2s^2 I)^{-\frac{1}{2}} = w \frac{1}{\sqrt{2s^2}} I$ for all point pairs, and $FRE_{weighted}$ and FRE_{std} (the FRE of the original ICP) are related by

$$FRE_{weighted}^2 = \frac{Nw^2}{2s^2} FRE_{std}. \quad (15)$$

Consequently, the two FREs and thus the convergence thresholds for the original ICP and the A-ICP are not comparable, although both algorithms should produce the same result in this case (isotropic, homogeneous noise).

While the choice of w has no influence on the corresponding points that are established or on the transformation that is computed by the corresponding point registration method, it may be used to normalize the weighted FRE. Setting it to

$$w = s \sqrt{\frac{2}{N}} \quad (16)$$

makes the convergence thresholds for the original ICP and the A-ICP directly comparable for this case of isotropic, homogenous noise. For the general case (anisotropic, inhomogenous localization errors), Danilchenkov and Fitzpatrick addressed the issue in the weighted corresponding points registration algorithm by requiring that

$$\sum_{i=1}^{N_X} \text{trace}(W_i W_i') = 3. \quad (17)$$

However, we cannot apply this principle because corresponding points may potentially change from one iteration to the next, and we need to make sure that the same FRE is minimized in the steps *establishing correspondences* and *computing the transformation*. One solution to this problem is to normalize the covariance matrices such that their traces are identical, as discussed in Section 4.3. This implies, however, that we cannot give less weight to those points with higher variance when computing the transformation. In order to be able to leave the covariances unmodified but still obtain comparable thresholds, we propose the following procedure. Initially, we compute the mean variances $\mu_X(\sigma^2)$ and $\mu_Y(\sigma^2)$ for both input point sets (each averaged over all three principal axes and all N_X/N_Y points). If we then set $s^2 = \frac{\mu_X(\sigma^2) + \mu_Y(\sigma^2)}{2}$, FRE_{std} and $FRE_{weighted}$ would again be related by 16 in the case of isotropic homogenous noise. Hence, if we set $w = s \sqrt{\frac{2}{N}}$, the convergence thresholds ϵ_{std} used for the original ICP roughly compares to the threshold $\epsilon_{weighted}$.

3.5 Trimmed Variant of the A-ICP

In its original form, the A-ICP requires the surface given by X to represent a part of the surface given by Y because a corresponding point is sought for each $x \in X$. In order to allow for registration of *partially overlapping* surfaces, we can modify the algorithm, following the idea of the trimmed ICP [28]. It is based on a parameter $\xi \geq 0$, called *minimum overlap*, which represents the minimum guaranteed portion of the data points that can be paired. After step 2 of the algorithm, we sort all weighted distances in increasing order and use only the best ξ percent correspondences as input for step 3 of the algorithm. It can be proven that the convergence properties are not affected by doing this because both steps of the algorithm still decrease the weighted FRE. If we were to apply the described trimmed version of the A-ICP without any further changes, however, there could be a bias toward points with high variance. Consider two point pairs (\vec{x}_i, \vec{z}_i) and (\vec{x}_j, \vec{z}_j) with the same euclidean distance $\|\vec{x}_i - \vec{z}_i\|_2 = \|\vec{x}_j - \vec{z}_j\|_2$ but a different weighted difference $d_{new}(\vec{x}_i, \vec{z}_i) < d_{new}(\vec{x}_j, \vec{z}_j)$ due to higher variances associated with the first point pair. In the original

version of the A-ICP, the pair with higher variance would contribute less to the transformation than the second pair, which is generally a desirable property. However, in the trimmed A-ICP, the sorting of the distances could potentially lead to exclusion of the potentially more reliable second point pair, while the first pair would be within the set of best pairs due to its smaller weighted distance. This issue can be addressed by performing a weight normalization as described in Section 4.3.

3.6 Runtime Optimization

As already mentioned in Section 2, one of the main drawbacks of the ICP is the quadratic complexity of establishing correspondences, which, however, can be reduced to $O(N_X \log N_Y)$ by applying *kd* trees. Unfortunately, this concept cannot be directly applied to the A-ICP because *weighted* distances are required. To make the correspondence search more efficient, we initialize the A-ICP with the (faster) original ICP to determine a good starting pose for the iterative refinement. Furthermore, we propose constraining the search of the weighted nearest neighbor to a certain radius r from the point of interest. For this purpose, step 2 of the proposed algorithm is modified such that weighted distances are only computed for pairs of points whose euclidean distance to each other is smaller than r . A *kd* tree is applied to determine those points $Y_i^k \subset Y$ that are located within a distance r to a given point $\vec{x}_i^k \in X^k$. If the weighted FRE is higher than in the previous iteration, the procedure is repeated with an increased radius $r := 2r$. This makes sure that $FRE_{weighted}$ never increases and convergence can still be guaranteed.

4 DERIVATION OF COVARIANCE MATRICES

As a reasonable choice of covariance matrices is crucial to the performance of the algorithm (remember that isotropic homogenous noise results in the original ICP), this section presents two representative detailed examples for deriving covariance matrices for a given application.

4.1 Accounting for Mesh Resolution

Let us assume that we want to rigidly register two surface meshes generated from two potentially different image modalities. As the original ICP implicitly assumes that the input point sets are observed with zero-mean, identical, and isotropic Gaussian noise, it requires corresponding points to correspond to the same physical location. This may lead to a suboptimal registration result, as illustrated in Fig. 1a. To compensate for this effect, we propose increasing the variance along the surface based on the Voronoi region of a point (cf., Figs. 1b and 3a). Intuitively speaking, our idea is as follows: Two points should get a small weighted distance if we can match them by moving them around within their Voronoi region. While a movement away from the original vertex position but along the surface should only result in a small increase in the distance, movements away from the surface should increase the distance significantly.

To define the covariance matrix for a point \vec{p} based on this idea, we need to determine three principal axes arranged in the columns of a matrix $V_{\vec{p}}$ and a diagonal matrix $S_{\vec{p}} = \text{diag}(\sigma_{\vec{p},1}, \sigma_{\vec{p},2}, \sigma_{\vec{p},3})$ with $\sigma_{\vec{p},j}$ representing the standard

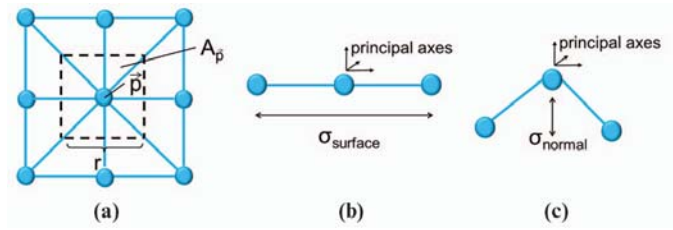


Fig. 3. (a) Vertex \vec{p} and its Voronoi region with area $A_{\vec{p}}$. After A-ICP-based registration with a second mesh, the vertex corresponding to \vec{p} should be located within the Voronoi region of \vec{p} . Hence, instead of forcing an exact matching of points upon computing the rigid registration, we allow a certain distance along the surface. (b) In flat regions, a movement perpendicular to the surface normal (represented by $\sigma_{surface}$) corresponds to a movement along the surface. (c) In general, however, a movement along the surface additionally requires a movement *along* the surface normal (represented by σ_{normal}).

deviation along the principal axis j ($\sigma_{\vec{p},1} \geq \sigma_{\vec{p},2} \geq \sigma_{\vec{p},3}$). The covariance matrix of \vec{p} can then be set to $\Sigma_{\vec{p}} = V_{\vec{p}} S_{\vec{p}}^2 V_{\vec{p}}'$. The following two paragraphs describe two different methods for defining $V_{\vec{p}}$ and $S_{\vec{p}}$. In both methods, one principal axis is set along the surface normal $n_{\vec{p}}$ with variance σ_{normal}^2 , while the two remaining principal axes are set perpendicular to $n_{\vec{p}}$ with variances $\sigma_{surface,1}^2$ and $\sigma_{surface,2}^2$.

4.1.1 Voronoi-Based Method for Covariance Matrix Computation (CM_VORONOI)

The two principal axes representing the localization error along the surface are set perpendicular to $n_{\vec{p}}$ in an arbitrary fashion and assigned the same variance $\sigma_{surface}^2 = \sigma_{surface,1}^2 = \sigma_{surface,2}^2$, which is derived from the Voronoi region of \vec{p} as follows: Consider two different vertices \vec{p}_i and \vec{p}_j , each located on a flat part of a mesh. Let us further assume the Voronoi areas $A_{\vec{p}_i}$ and $A_{\vec{p}_j}$ to be approximately square-shaped, with edge length $r_i = \sqrt{A_{\vec{p}_i}}$ and $r_j = \sqrt{A_{\vec{p}_j}}$, as illustrated in Fig. 3a. Now, if r_i and r_j are related by a constant c , i.e., $r_i = c \cdot r_j$, we want the standard deviations along the surface, $\sigma_{surface}(\vec{p}_i)$ and $\sigma_{surface}(\vec{p}_j)$, to be related by the same factor. This can be achieved by setting the sum of the variances $\sigma_{surface}^2$ for each vertex \vec{p} proportional to $A_{\vec{p}}$:

$$\sigma_{surface}^2 + \sigma_{surface}^2 = \beta^2 A_{\vec{p}}, \quad (18)$$

where β is a scaling factor because this implies $\sigma_{surface} = \frac{\beta}{\sqrt{2}} r$. The standard deviations of the vertices from our example, $\sigma_{surface}(\vec{p}_i)$ and $\sigma_{surface}(\vec{p}_j)$, would thus be related by

$$\sigma_{surface}(\vec{p}_i) = \frac{\beta}{\sqrt{2}} r_i = \frac{\beta}{\sqrt{2}} c \cdot r_j = c \cdot \sigma_{surface}(\vec{p}_j). \quad (19)$$

If we assume our mesh to be noise free, we could further set $\sigma_{normal} = 0$. It is well known that the trace of a square matrix equals the sum of its eigenvalues; hence, the trace of a covariance matrix equals the sum of the variances along the individual principal axes. Consequently, (18) requires the trace of $\Sigma_{\vec{p}}$ to be proportional to the Voronoi area:

$$\text{trace}(\Sigma_{\vec{p}}) = \beta^2 A_{\vec{p}}. \quad (20)$$

Let us now generalize this idea to the case where the Voronoi region of a point \vec{p} is not necessarily located on a plane. In the previous example, our idea was to account for the high-localization error along the surface by using a high

variance in the direction perpendicular to the surface normal. While this procedure is reasonable in flat surface regions, it does not produce the desired result in regions with high curvature, as illustrated in Fig. 3. The reason is that if we move a point strictly perpendicularly to the surface normal, we do not really stay on the surface. For this reason, we introduce a scaling factor $\alpha \in [0; 1]$ which relates the variance along the surface normal σ_{normal}^2 with the variance along the surface $\sigma_{surface}^2$: $\sigma_{normal} = \alpha \cdot \sigma_{surface}$. Typically, we will set α to a value close to 0, indicating that the localization error occurs primarily perpendicularly to the surface normal. Alternatively, α can be set individually for each vertex, based on the curvature at that point, for example. Motivated by the example related to Fig. 3a, we keep the Voronoi area as a measure of the variance in a vertex \vec{p} by requiring 20 to hold. Due to this normalization, we can initialize $\sigma_{surface}$ with an arbitrary value, e.g., $\sigma_{surface} = 1$ mm. It is worth noting that if the same method for covariance computation is used for both input meshes, the scaling factor β has no influence on the registration result and can thus be set to a standard value $\beta = 1$.

4.1.2 Principal Component Analysis (PCA)-Based Method for Covariance Matrix Computation (CM_PCA)

The previous method uses arbitrary axes along the surface. The aim of this method for covariance computation is to account for different spreads of neighboring vertices in different directions as follows: One principal axis of localization error is set in the direction of the surface normal $n_{\vec{p}}$ and all vertices in the closed neighborhood of \vec{p} are projected onto the plane with normal $n_{\vec{p}}$ that passes \vec{p} . Next, a PCA is performed on the projected points to obtain the second and third principal axes of localization error. The variance representing the localization error along a given principal axis is then set to the variance obtained from projecting all vertices in the closed neighborhood of \vec{p} onto that axis and multiplied by a scaling factor β . Again, if the same method for covariance computation is used for meshes, the scaling factor β has no influence on the registration result and can thus be set to a standard value $\beta = 1$.

4.2 Accounting for Noise in Time-of-Flight (ToF) Cameras (CM_TOF)

It is well known that range cameras (e.g., ToF cameras) have a much higher localization uncertainty in the direction of view of the camera than orthogonal to that direction [8]. Based on the standard pin-hole camera model, this issue can be accounted for by setting the first principal axis of noise along the ray connecting the imaged object point \vec{x} to the center of the associated chip pixel (on the image plane) and assigning a high variance σ_{ray}^2 in that direction. The remaining two principal axes are set orthogonal to that ray (in an arbitrary fashion) with a small variance $\sigma_{lateral}^2$. The standard deviation σ_{ray} along the ray can, for example, be set to a constant value depending on the distance of the object being examined from the camera or be estimated from a set of distance images as described in [41]. This method for covariance computation will be referred to as CM_TOF. It will typically be combined with one of the methods for covariance matrix computation described previously when matching a ToF surface to a

reference surface. In this case, the scaling factor β of CM_VORONOI and CM_PCA weighs the influence of the covariance matrices addressing mesh resolution relative to the influence of the covariance matrices addressing the noise in ToF cameras.

4.3 Normalization of Covariance Matrices

All of the methods described for covariance computation potentially lead to an unequal distribution of variances among the points. As a higher variance decreases the weighted distance between points, this effect may not be desirable. For example, in the trimmed version of the A-ICP, there would be a bias toward points with high variance, as discussed in Section 3.4. One way to overcome this issue to some extent is to normalize the covariance matrices such that they represent the same amount of variance. As already mentioned above, the trace of a covariance matrix equals the sum of the variances along the individual principal axes. We can thus normalize the covariance matrices by requiring their traces to be identical:

$$\text{trace}(\Sigma_{\vec{p}}) = c \quad \vec{p} \in X \cup Y. \quad (21)$$

This implies that we assume the localization error in \vec{p} , often referred to as fiducial localization error (FLE), to be the same for all points \vec{p} (i.e., $\langle FLE_{\vec{p}}^2 \rangle = \text{trace}(\Sigma_{\vec{p}}) = c$), while we allow their anisotropies to vary. Furthermore, the normalization has another desirable side effect. As already mentioned in Section 3.4, the size of the weighted FRE is somewhat arbitrary because it decreases with increasing variances. Let us now assume that we normalize all covariance matrices such that their traces are equal to c . The mean variance averaged over all points $\vec{x} \in X$ and all their principal axes will then be

$$\mu_{\sigma^2}(X) = \frac{1}{3N_X} \sum_{i=1}^{N_X} \sum_{k=1}^3 \sigma_{x_{ik}}^2 = \frac{1}{3N_X} \sum_{i=1}^{N_X} \text{trace}(\Sigma_{\vec{x}_i}) = \frac{c}{3}. \quad (22)$$

Analogously, one can show that the mean variance $\mu_{\sigma^2}(Y)$ averaged over all points $\vec{y} \in Y$ is $\frac{c}{3}$. Consequently, if we set $w = \sqrt{\frac{2c}{3N}}$, we obtain comparable convergence thresholds for the ICP and the A-ICP.

5 EXPERIMENTS AND RESULTS

We performed a range of experiments to evaluate the performance of our algorithm in the context of whole surface registration (Section 5.1), partial surface registration (Section 5.2), and registration of partially overlapping surfaces (Sections 5.3 and 5.4). Furthermore, the runtime of the algorithm (Section 5.5) and its convergence properties (Section 5.6) were assessed. For all experiments, we used our own C++-based implementation of the A-ICP, which was successfully integrated into the *Medical Imaging Interaction Toolkit (MITK)* (www.mitk.org). The implementation of the original ICP by *The Visualization Toolkit (VTK)*, which makes use of *k-d-trees* [32] for correspondence search, served as a basis for comparison.

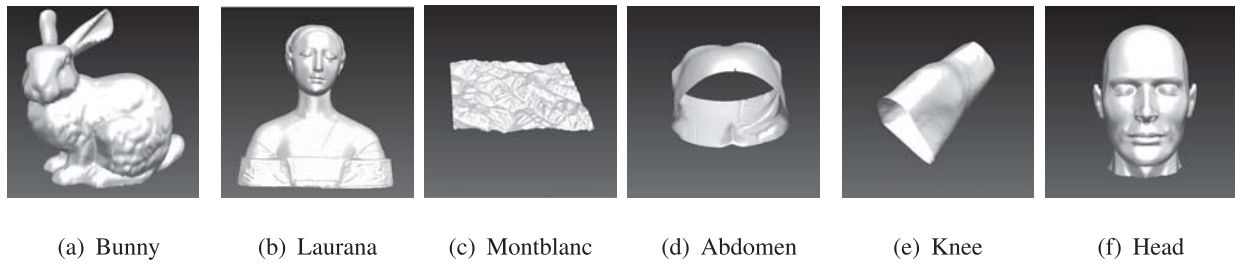


Fig. 4. Meshes used for the experiments.

5.1 Whole Surface Registration

In this experiment, we used publicly available surface meshes from three different shapes: the well-known Stanford *Bunny*,² the statue *Laurana*,³ and a landscape, referred to as *Montblanc*⁴ (cf., Fig. 4). All meshes were moved to the origin and (if necessary) scaled such that they had realistic sizes in *mm*.⁵ For each shape, a set of targets distributed within the object were then defined and two different decimations, consisting of approximately 1,000 and 3,000 vertices, respectively, were generated with the quadric edge collapse decimation method provided by MeshLab.⁶ Let $T(x, y)$ denote the rigid transformation that represents a translation by x along each coordinate axis and a rotation about y about each axis. In this experiment, the transformation $T(20 \text{ mm}, 20^\circ)$ was applied to the higher resolution meshes (i.e., the ones with 3,000 vertices) of the *Bunny* and *Laurana* while $T(20 \text{ m}, 20^\circ)$ was applied to *Montblanc*.

Both the original ICP and the A-ICP (with initialization by the ICP) were then applied to register different surfaces of the same shape in pairs. The A-ICP was applied with both methods of covariance computation introduced in Section 4.1. For this purpose, the parameter α for CM_VORONOI was varied from 0 to 1. Note that a variation of the scaling factor β would not yield different results, because we use the same method for covariance computation for both input shapes. The convergence threshold ϵ was set to 10^{-5} m for *Montblanc* and to 10^{-5} mm for the two other shapes. We performed a normalization of the weighted FRE according to Section 3.4 in order to make the thresholds for the ICP and the A-ICP comparable. After convergence of the algorithms, the target registration error (TRE), which we defined as the RMS distance between the estimated target position and the corresponding ground truth position, was determined. The same experiment was then performed with noisy variants of the applied meshes. For this purpose, we applied Gaussian noise along all vertex normals, using a standard deviation of 1 m for *Montblanc* and of 1 mm for both other shapes.

The results of the experiments with whole surfaces are presented in Figs. 5 and 6. The mean decrease in TRE averaged over all meshes was 78 percent (CM_VORONOI,

$\alpha = 0.1$) and 72 percent (CM_PCA) in the case of the ideal meshes and 56 percent (CM_VORONOI, $\alpha = 0.3$) and 50 percent (CM_PCA) for the noisy meshes. Fig. 6 further shows the results for the CM_VORONOI method as a function of the parameter $\alpha \in [0; 1]$. The mean number of iterations required by the original ICP was 48 (without noise) and 49 (with noise), while the A-ICP used an additional number of six iterations averaged over all cases.

5.2 Partial Surface Registration

One of the key challenges related to computer-assisted medical interventions is the registration of intraoperative patient data with preoperative data. One increasingly popular approach to achieve this is to acquire surface data during the intervention using a laser scanner [3], for example, and to match the resulting partial surface mesh with a corresponding mesh extracted from 3D medical imaging data.

In this experiment, we used three data sets generated from human bodies: an *Abdomen* and a *Knee* segmented from computed tomography (CT) data, as well as the *Head* of a publicly available *Torso*⁷ (cf., Fig. 4). For each mesh, an ideal ToF image was created with an approximately ventral view of the camera on the patient. Based on the ideal depth map, a noisy partial surface was generated with the simulation framework presented in [41]. All reference meshes were then decimated so that they featured about 2,500 vertices and transformed with the transformation $T(20 \text{ mm}, 20^\circ)$. In the case of the *Abdomen* and the *Knee*, the partial surfaces were cut to ensure that only part of the visible body parts' surfaces was captured with the virtual ToF camera, which led to a more challenging registration task. Both, the original ICP and the A-ICP (with initialization by the ICP) were then applied to register the partial ideal and noisy ToF surfaces with the whole surfaces. In the case of the ideal images, the methods CM_PCA and CM_VORONOI were used for both methods with the default parameter $\alpha = 0.1$. For the noisy ToF surfaces, the CM_PCA method (used for both meshes) and the CM_TOF method combined with CM_VORONOI or CM_PCA were applied. For CM_TOF, the standard deviation along the camera ray for a given object distance was obtained from the simulation framework described in [41], while $\sigma_{lateral}$ was set to 0.1 mm as proposed in [41]. Furthermore, CM_VORONOI and CM_PCA were used for the reference surfaces with the default values $\beta = 2$ for homogenous surfaces (here: *Skin* and *Knee*) and $\beta = 1$ for surfaces

2. Provided by Stanford University Computer Graphics Laboratory, <http://graphics.stanford.edu/data/3Dscanrep/>.

3. Provided by the Institute of Information Science and Technologies (ISTI, Pisa, Italy).

4. Provided courtesy of DISI (Department of Computer and Information Science, University of Genova, Italy) by the AIM@SHAPE Shape Repository.

5. The original shapes are provided without units and fit into the unit sphere.

6. meshlab.sourceforge.net.

7. Provided courtesy of Alexandre Olivier-Mangon and George Drettakis (Institut National de Recherche en Informatique et en Automatique (INRIA), Nice, France) by the AIM@SHAPE Shape Repository, <http://shapes.aim-at-shape.net>.

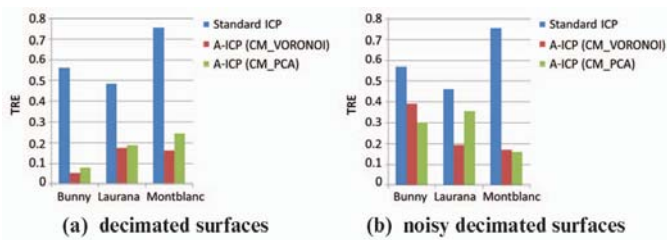


Fig. 5. Results for whole surface registration. The TRE for a set of targets distributed within the surfaces is given in mm for the *Bunny* and *Laurana* and in m for *Montblanc*.

featuring curved regions (here: *Head*). Note in this context that the problem illustrated in Fig. 2a occurs primarily in curved regions. Again, we performed a normalization of the weighted FRE according to Section 3.4 and used a convergence threshold of $\epsilon = 10^{-5}$ mm for both methods. After convergence of the algorithms, the TRE was determined as in the previous experiment.

The results of this experiment are given in Fig. 7. The mean decrease in TRE averaged over all meshes without noise was 86 percent for both methods (CM_VORONOI and CM_PCA). In the case of the noisy ToF images, the mean decrease in TRE ranged from 68 to 80 percent. The mean number of iterations required by the original ICP for these experiments was 122 (ideal) and 136 (noisy). Application of the A-ICP required an additional number of 15 (CM_VORONOI) and 16 (CM_PCA) iterations for the ideal meshes and an additional number of 28 (CM_TOF and CM_VORONOI), 35 (CM_TOF and CM_PCA), and 42 (CM_PCA and CM_PCA) iterations in the case of the noisy meshes.

5.3 Registration of Partially Overlapping Surfaces

Many applications require registration of partially overlapping surfaces. For example, if we look at our previous example, the range image of the *Abdomen* or the *Knee* may potentially represent a larger portion of the body than the CT image. To address this issue, we cut the reference shapes such that only a partial overlap between the ToF surfaces and the reference surfaces was obtained, as shown in Fig. 9c.

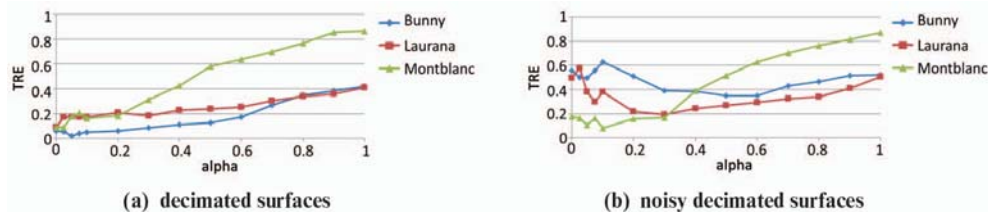


Fig. 6. Results for the A-ICP applied to the whole surfaces. The TRE is shown in mm (*Bunny*, *Laurana*) and m (*Montblanc*) as a function of the parameter $\alpha = \frac{\sigma_{normal}}{\sigma_{surface}}$.

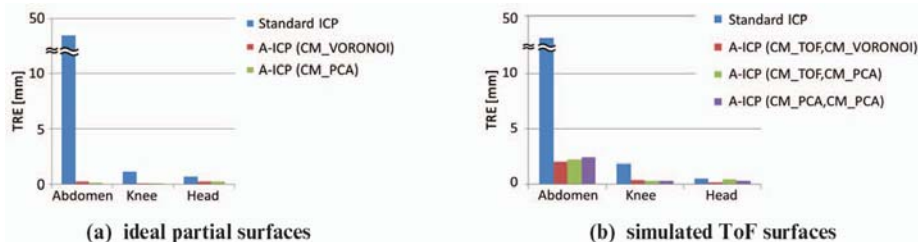


Fig. 7. Results for partial surface registration. The TRE for a set of targets distributed within the reference meshes is given for both (a) the ideal ToF images without noise and (b) the physically realistic noisy ToF surfaces.

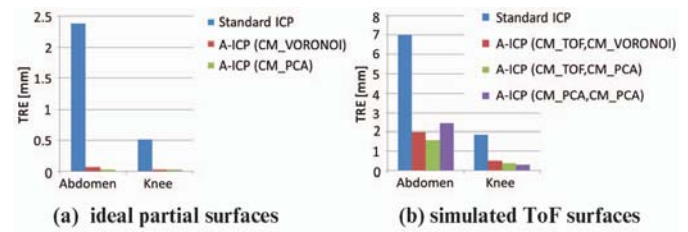


Fig. 8. Results for partially overlapping surface registration. The TRE for a set of targets distributed within the reference meshes is given for both (a) the ideal ToF images without noise and (b) the physically realistic noisy ToF surfaces.

The experiment described in the previous section was then repeated with trimmed versions (overlap: 70 percent for the *Abdomen* and 50 percent for the *Knee*) of the ICP and the A-ICP. All methods were applied with and without covariance normalization (cf., Section 3.4).

The results of this experiment are shown in Fig. 8. The mean decrease in TRE averaged over all meshes without noise was about 96 percent. In the case of the noisy ToF images, the mean decrease in TRE ranged from 72 to 79 percent. For the normalized variant, we obtained similar results (not shown here). The mean number of iterations required by the original ICP for these experiments was 578 (ideal) and 552 (noisy). Application of the A-ICP required an additional number of 5 (CM_VORONOI) and 7 (CM_PCA) iterations for the ideal meshes and an additional number of 19 (CM_TOF and CM_VORONOI), 18 (CM_TOF and CM_PCA), and 39 (CM_PCA and CM_PCA) iterations in the case of the noisy meshes. Fig. 9 shows a registration result for the *Abdomen* with 50 percent overlap.

5.4 Stitching

One important application for registration of partially overlapping surfaces is the reconstruction of a 3D model from a set of range images, also referred to as *stitching*. To evaluate the performance of the A-ICP algorithm for this purpose, we simulated three range images of the statue *Laurana*, representing a pose of -90 , 0 , and 90 degrees

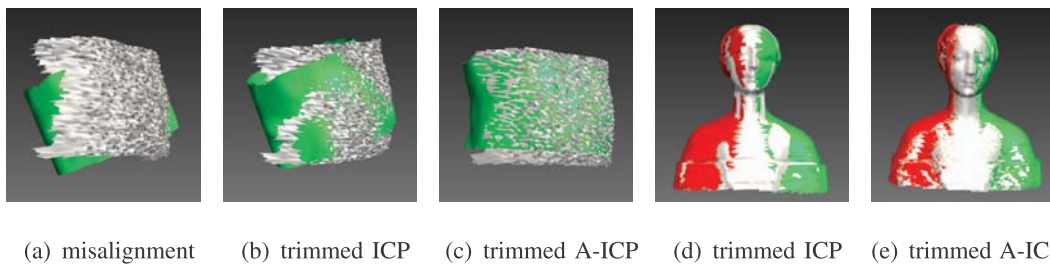


Fig. 9. (a)-(c) Registration of noisy mesh generated from simulated ToF range data to a reference mesh of a human abdomen using the trimmed version of the ICP and the A-ICP with $\xi = 50$ percent. (a) Initial misalignment after application of the transformation $T(20 \text{ mm}, 20^\circ)$, (b) registration result after application of the ICP, and (c) result after application of the A-ICP. (d)-(e) Stitching result for (d) the original ICP and (e) the A-ICP with method CM_PCA for covariance computation. The red and green range images were registered to the white one.

relative to the virtual range camera. We then applied the trimmed version of the ICP and A-ICP for registering the partial surfaces using an overlap of $\xi = 30$ percent. The results are shown in Figs. 9d and 9e. Application of the A-ICP led to a decrease of the TRE by 97 percent (CM_PCA, TRE 0.3 mm) and 98 percent (CM_PCA, normalized, TRE 0.2 mm) compared to the original ICP (TRE 9 mm).

5.5 Runtime Assessment

To demonstrate the suitability of our method for runtime optimization, we repeated two of the previous experiments (whole surface registration with the *Bunny* and partial surface registration with the *Head*) with a varying search radius. Registration of the *Bunny* (approximately 1,000 and 3,000 vertices) took 200 s without runtime optimization and 600 ms with runtime optimization (search radius: 1 cm). Registration of the *Head* (about 5,000 and 2,500 vertices) took 1,650 s (i.e., about 28 min.) versus 6 s. In both cases, this corresponds to a decrease in runtime by a factor > 100 . The corresponding computing times for the original ICP were approximately 100 and 800 ms, respectively. Fig. 10 shows the mean time per iteration of the A-ICP with runtime optimization as a function of the search radius for both meshes.

5.6 Convergence

In the above experiments, we always initialized the A-ICP with the original ICP algorithm for the purpose of runtime optimization. To demonstrate the favorable convergence properties of the A-ICP, we repeated some of the experiments described in Sections 5.1-5.3 without ICP initialization and with different initial alignments $T(x \text{ mm}, x^\circ)$ (c.f., Section 5.1). We used the *Bunny* without noise for whole surface registration, the *Abdomen* for partial surface registration, and the *Knee* for registration of partially overlapping surfaces. Starting with no misalignment, i.e., $x = 0$, we successively increased x by 10 (millimeters and degrees, respectively) until both the original and the A-ICP, failed to converge to a pose

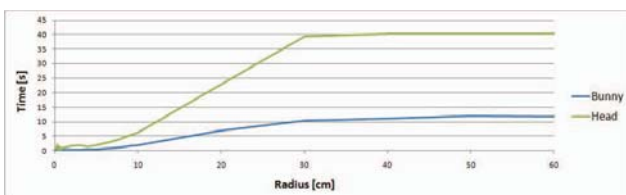


Fig. 10. Mean time per iteration as a function of the search radius.

close to the optimum ($TRE < 10$ mm). For the A-ICP, we used the covariance method CM_PCA for both shapes in all experiments and no search radius. The results of the experiment, presented in Table 1, show that the A-ICP is much more robust with respect to the initial misalignment. Furthermore, it requires considerably fewer iterations (typically 50 percent less).

6 DISCUSSION

In this paper, we presented a variant of the ICP that accounts for anisotropic and inhomogeneous localization errors. We showed how to normalize the defined weighted FRE such that it is comparable to the FRE of the original ICP and proved that the defined cost function decreases in every iteration. Furthermore, we described how to apply the algorithm for robust fine registration of surface meshes. An evaluation using publicly available surface meshes as well as a set of meshes extracted from medical imaging data showed a dramatic increase in accuracy compared to the original ICP, especially in the case of partial surface registration.

The two methods for accounting for mesh resolution, namely, CM_VORONOI and CM_PCA, yielded similar results. The main advantage of the PCA-based method is that it accounts for different spreads of the vertices along the surface and that it requires no parameters. Furthermore, it is potentially more robust to noise because it adjusts the variance along the surface normal depending on the distribution of the vertices. The Voronoi-based method, on the other hand, is simple to implement and computationally very efficient. Despite the excellent results of both methods, one might argue that in this particular scenario, it would make more sense to use the covariance matrices for computation of the transformation only, and apply the standard euclidean distance for establishment of correspondences because the covariance matrices do not actually represent noise in the data (cf., Fig. 1a). In that case, however, there would no longer be any guarantee of convergence of the algorithm. One possibility to address this issue is to normalize all covariance matrices such that they represent the same amount of variance as described in Section 4.3. However, we did not generally obtain better results with this method. In fact, not even in the case of the trimmed A-ICP did the normalization yield an improvement. One possible explanation for this is that point pairs with high variance contribute more to the transformation after the normalization process, which is generally not desirable. Hence, this

TABLE 1
Results for the Convergence Experiment Showing the TRE (in mm) and the Number of Iterations in “()”
for Different Shapes and Different Initial Misalignments

Shape	Method	T0	T10	T20	T30	T40	T50	T60	T70	T80	T90
<i>Bunny</i>	ICP	0.3(14)	0.6(27)	0.6(35)	0.4(38)	0.6(42)	0.5(50)	0.5(53)	0.5(58)	0.5(92)	-
	A-ICP	0.1(7)	0.1(14)	0.1(16)	0.1(20)	0.1(24)	0.1(27)	0.1(33)	0.1(38)	0.1(46)	0.1(52)
<i>Abdomen</i>	ICP	1.9(41)	-	-	-	-	-	-	-	-	-
	A-ICP	1.0(7)	1.4(90)	2.4(110)	-	-	-	-	-	-	-
<i>Knee</i>	ICP	0.3(16)	1.5(193)	1.5(370)	-	-	-	-	-	-	-
	A-ICP	0.4(19)	0.4(83)	0.3(145)	0.4(245)	0.4(305)	0.4(329)	0.4(348)	-	-	-

“-”represents a TRE > 10 mm.

negative effect may cancel out the positive effect of the normalization on the selection of correspondences.

When registering ToF data, the ToF specific method CM_TOF combined with CM_PCA or CM_VORONOI yielded results similar to those yielded by the PCA method applied to both surfaces. The results were similar, although the noise in the ToF data was modeled quite accurately [41]. One possible explanation for this phenomenon is the fact that the CM_TOF method requires a scaling factor β to be set for the covariance method of the reference surface. Although the registration result was very robust with respect to the choice of β , we observed that with the optimal β , CM_TOF could always outperform CM_PCA. Further investigation of the parameter could thus lead to an even better registration result. On the other hand, the CM_TOF method is rather complicated compared to the CM_PCA method, for example, because it requires the intrinsic camera parameters of the device that was used to record the data as well as the noise characteristics of the camera as input. Note, in this context, that CM_PCA could readily be applied to range data obtained from a different modality without specifying the error characteristics (e.g., a structured light system, which typically yields higher errors in camera direction as well). Furthermore, CM_TOF cannot be applied for registering two (partially overlapping) ToF surfaces because in the current version, the resolution of the ToF mesh is not taken into account. Note that the intervertex distance in surfaces generated from ToF range images generally increases with 1) an increasing angle of the surface relative to the image plane, 2) an increasing distance of the object under observation from the camera, and 3) an increasing distance from the ray representing the center pixel. For all these reasons, we recommend the CM_PCA method for registration of ToF data.

Despite the promising results of our study, one might argue that one could obtain similar results for the original ICP by upsampling and denoising the meshes. Although this would be computationally expensive, the runtime of the ICP with these improvements might still be better than that of the A-ICP. While this is a valid objection, it is only relevant to some extent because 1) as we are dealing with discrete surface data, there will always be some remaining uncertainty along the surface that is worth being accounted for, and 2) there is a lot of room for improving runtime. The most

obvious extension is the parallelization of the nearest neighbor search based on a GPU implementation. Furthermore, the multicore technology of state-of-the-art personal computers could be used to parallelize various modules of the software (computation/propagation of covariance matrices, transformation of moving points, etc.). In addition, the convergence threshold for the original ICP could be increased, reflecting the fact that we do not need an optimum registration result with respect to the unweighted FRE, but only a good guess at initialization of the A-ICP. Similarly, in each iteration, the convergence threshold for the weighted corresponding point registration (cf., Section 3.2) could be increased because we do not necessarily need an optimal transformation while the correspondences are changing. Alternatively, decreasing the maximum number of iterations of the weighted corresponding point algorithm could decrease the runtime. Furthermore, it should be noted that weighting matrices computed by the corresponding point registration algorithm in iteration k can be reused for nearest neighbor computation in iteration $k + 1$ of the A-ICP. Finally, as the proposed method is able to account for the mesh resolution, it is potentially robust to downsampling of meshes, which, in turn, would decrease runtime. Based on these optimizations, it may even be beneficial to apply the A-ICP without initialization by the ICP (which is currently done for the purpose of runtime optimization). In fact, our experiments show that the convergence properties of the A-ICP are generally better than that of the original ICP with respect to the number of iterations.

It is worth mentioning that this paper investigated registration of meshes that essentially represented the same shapes—deformations or systematic errors have not yet been taken into account. Hence, future work includes rigid registration of meshes that are subject to systematic errors. Furthermore, it could be argued that we should have compared the A-ICP to one of the more recently proposed variants of the ICP as opposed to the *original* one. One reason for this was that convergence played an important role in the development of our algorithm, and only very few ICP variants can be guaranteed to converge. Those that do have not generally been designed to address anisotropic localization errors. Nevertheless, we are planning to compare our algorithm with different variants of the ICP (e.g., [21]) as well as with other methods proposed for fine surface registration (e.g., [42]) in an application-specific manner, i.e., with the aim

of selecting the best performing algorithm for a given application. For this purpose, our software will be available for download upon publication of this paper at www.mtk.org/wiki/projects/AnisotropicICP.

In conclusion, we proposed a generalization of the ICP that keeps the main advantages of the original ICP algorithm, namely, the guaranteed convergence, the general applicability in various fields, and the straightforward implementation, while targeting one of the key issues: the assumption of isotropic localization errors in the input data. In all our experiments, registration accuracy was improved considerably, which confirms the robustness of the method. Because of its flexibility in incorporating prior knowledge, its convergence properties, and the dramatic improvement in accuracy compared to the original ICP, we consider our generalization of the ICP to be an important work in the context of fine surface registration. As point-based surface registration is a central component in various settings, the potential impact of the proposed method on future applications is high.

ACKNOWLEDGMENTS

The authors would like to thank U. Rietdorf, M. Engel, and A. Seitel (DKFZ) as well as B. Radeleff and C. Sommer (University of Heidelberg) for providing the medical imaging data. This work was supported by the German Research Foundation (DFG, PD 15577).

REFERENCES

- [1] P. Yan and K.W. Bowyer, "Biometric Recognition Using Three-Dimensional Ear Shape," *IEEE Trans. Pattern Analysis and Machine Intelligence*, vol. 29, no. 8, pp. 1297-1308, Aug. 2007.
- [2] L. Armesto, J. Minguez, and L. Montesano, "A Generalization of the Metric-Based Iterative Closest Point Technique for 3D Scan Matching," *Proc. IEEE Int'l Conf. Robotics and Automation*, pp. 1367-1372, 2010.
- [3] D.M. Cash, M.I. Miga, S.C. Glasgow, B.M. Dawant, L.W. Clements, Z. Cao, R.L. Galloway, and W.C. Chapman, "Concepts and Preliminary Data Toward the Realization of Image-Guided Liver Surgery," *J. Gastrointestinal Surgery*, vol. 11, pp. 844-859, 2007.
- [4] E.M. Bispo and R.B. Fisher, "Free-Form Surface Matching for Surface Inspection," *Proc. Sixth IMA Conf. Math. of Surfaces*, pp. 119-136, 1994.
- [5] O. van Kaick, H. Zhang, G. Hamarneh, and D. Cohen-Or, "A Survey on Shape Correspondence," *Computer Graphics Forum*, vol. 30, no. 6, pp. 1681-1707, 2011.
- [6] P.J. Besl and N.D. McKay, "A Method for Registration of 3D Shapes," *IEEE Trans. Pattern Analysis and Machine Intelligence*, vol. 14, no. 2, pp. 239-256, Feb. 1992.
- [7] Y. Chen and G. Medioni, "Object Modeling by Registration of Multiple Range Images," *Int'l J. Computer Vision and Image Understanding*, vol. 10, pp. 145-155, 1992.
- [8] R. Lange, "3D Time-of-Flight Distance Measurement with Custom Solid-State Image Sensors in CMOS/CCD-Technology," PhD thesis, Univ. of Siegen, 2000.
- [9] R. Balachandran and J.M. Fitzpatrick, "Iterative Solution for Rigid-Body Point-Based Registration with Anisotropic Weighting," *Proc. SPIE*, vol. 7261, no. 1, pp. 72613D-1-72613D-10, 2009.
- [10] R.S.J. Estépar, A. Brun, and C.-F. Westin, "Robust Generalized Total Least Squares Iterative Closest Point Registration," *Proc. Medical Image Computing and Computer-Assisted Intervention*, pp. 234-241, 2004.
- [11] N. Ohta and K. Kanatani, "Optimal Estimation of Three-Dimensional Rotation and Reliability Evaluation," *Proc. Fifth European Conf. Computer Vision*, pp. 175-187, 1998.
- [12] L. Maier-Hein, T.R. dos Santos, A.M. Franz, H.-P. Meinzer, and J.M. Fitzpatrick, "Iterative Closest Point Algorithm with Anisotropic Weighting and Its Application to Fine Surface Registration," *Proc. SPIE*, vol. 7962, pp. 79620 W-1-79620 W-9, 2011.
- [13] S. Rusinkiewicz and M. Levoy, "Efficient Variants of the ICP Algorithm," *Proc. Third Int'l Conf. 3D Digital Imaging and Modeling*, pp. 145-152, 2001.
- [14] G. Turk and M. Levoy, "Zipped Polygon Meshes from Range Images," *Proc. ACM Siggraph*, pp. 311-318, 1994.
- [15] T. Masuda, K. Sakaue, and N. Yokoya, "Registration and Integration of Multiple Range Images for 3D Model Construction," *Proc. 13th Int'l Conf. Pattern Recognition*, pp. 879-883, 1996.
- [16] S. Weik, "Registration of 3D Partial Surface Models Using Luminance and Depth Information," *Proc. Int'l Conf. Recent Advances in 3D Digital Imaging and Modeling*, pp. 93-100, 1997.
- [17] G. Godin, M. Rioux, and R. Baribeau, "Three-Dimensional Registration Using Range and Intensity Information," *Proc. SPIE*, vol. 2350, pp. 279-290, 1994.
- [18] J. Feldmar and N. Ayache, "Rigid, Affine and Locally Affine Registration of Free-Form Surfaces," *Int'l J. Computer Vision*, vol. 18, no. 2, pp. 99-119, 1996.
- [19] G.C. Sharp, S.W. Lee, and D.K. Wehe, "ICP Registration Using Invariant Features," *IEEE Trans. Pattern Analysis and Machine Intelligence*, vol. 24, no. 1, pp. 90-102, Jan. 2002.
- [20] K. Pulli, "Multiview Registration for Large Data Sets," *Proc. Second Int'l Conf. 3D Digital Imaging and Modeling*, pp. 160-168, 1999.
- [21] S. Granger, X. Pennec, and A. Roche, "Rigid Point-Surface Registration Using an EM Variant of ICP for Computer Guided Oral Implantology," *Proc. Fourth Int'l Conf. Medical Image Computing and Computer-Assisted Intervention*, pp. 752-761, 2001.
- [22] S. Kaneko, T. Kondo, and A. Miyamoto, "Robust Matching of 3D Contours Using Iterative Closest Point Algorithm Improved by M-Estimation," *Pattern Recognition*, vol. 36, pp. 2041-2047, 2003.
- [23] G. Blais and M.D. Levine, "Registering Multiview Range Data to Create 3D Computer Objects," *IEEE Trans. Pattern Analysis and Machine Intelligence*, vol. 17, no. 8, pp. 820-824, Aug. 1995.
- [24] P.J. Neugenbauer, "Geometrical Cloning of 3D Objects via Simultaneous Registration of Multiple Range Images," *Proc. Int'l Conf. Shape Modeling and Applications*, pp. 130-139, 1997.
- [25] C. Dorai, G. Wang, A.K. Jain, and C. Mercer, "Registration and Integration of Multiple Object Views for 3D Model Construction," *IEEE Trans. Pattern Analysis and Machine Intelligence*, vol. 20, no. 1, pp. 83-89, Jan. 1998.
- [26] M.F. Hansen, M.R. Blas, and R. Larsen, "Mahalanobis Distance Based Iterative Closest Point," *Proc. SPIE*, vol. 6512, p. 65121Y, Feb. 2007.
- [27] P.C. Mahalanobis, "On the Generalized Distance in Statistics," *Proc. Nat'l Inst. of Science of Calcutta*, vol. 2, pp. 49-55, 1936.
- [28] D. Chetverikov, D. Stepanov, and P. Krsek, "Robust Euclidean Alignment of 3D Point Sets: The Trimmed Iterative Closest Point Algorithm," *Image and Vision Computing*, vol. 23, pp. 299-309, 2005.
- [29] B.K.P. Horn, "Closed-Form Solution of Absolute Orientation Using Unit Quaternions," *J. Optical Soc. Am. A*, vol. 4, pp. 629-642, 1987.
- [30] A.E. Johnson and S.B. Kang, "Registration and Integration of Textured 3D Data," *Proc. Int'l Conf. Recent Advances in 3D Digital Imaging and Modeling*, pp. 234-241, 1997.
- [31] T. Jost and H. Hügli, "A Multi-Resolution ICP with Heuristic Closest Point Search for Fast and Robust 3D Registration of Range Images," *Proc. Fourth Int'l Conf. 3D Digital Imaging and Modeling*, pp. 427-433, 2003.
- [32] D. Simon, "Fast and Accurate Shape-Based Registration," PhD thesis, Robotics Inst., Carnegie Mellon Univ., Dec. 1996.
- [33] G.P. Penney, P.J. Edwards, A.P. King, J.M. Blackall, P.G. Batchelor, and D.J. Hawkes, "A Stochastic Iterative Closest Point Algorithm (StochasticICP)," *Proc. Fourth Int'l Conf. Medical Image Computing and Computer-Assisted Intervention*, pp. 762-769, 2001.
- [34] T. Tamaki, M. Abe, B. Raytchev, and K. Kaneda, "Softassign and EM-ICP on GPU," *Proc. First Int'l Conf. Networking and Computing*, pp. 179-183, 2010.
- [35] C. Langis, M. Greenspan, and G. Godin, "The Parallel Iterative Closest Point Algorithm," *Proc. Third Int'l Conf. 3D Digital Imaging and Modeling*, pp. 195-202, 2001.
- [36] B. Combès and S. Prima, "Prior Affinity Measures on Matches for ICP-Like Nonlinear Registration of Free-Form Surfaces," *Proc. IEEE Sixth Int'l Conf. Symp. Biomedical Imaging*, pp. 370-373, 2009.

- [37] D. Münch, B. Combès, and S. Prima, "A Modified ICP Algorithm for Normal-Guided Surface Registration," *Proc. SPIE*, vol. 7623, no. 7, pp. 76231A-1-76231A-8, 2010.
- [38] H. Chui and A. Rangarajan, "A New Point Matching Algorithm for Non-Rigid Registration," *Computer Vision and Image Understanding*, vol. 89, pp. 114-141, Feb. 2003.
- [39] B. Amberg, S. Romdhani, and T. Vetter, "Optimal Step Nonrigid ICP Algorithms for Surface Registration," *Proc. IEEE Conf. Computer Vision and Pattern Recognition*, 2007.
- [40] A. Danilchenko and J. Fitzpatrick, "General Approach to First-Order Error Prediction in Rigid Point Registration," *IEEE Trans. Medical Imaging*, vol. 30, no. 3, pp. 679-693, Mar. 2011.
- [41] L. Maier-Hein, M. Schmidt, A. Franz, T. dos Santos, A. Seitel, B. Jähne, J. Fitzpatrick, and H. Meinzer, "Accounting for Anisotropic Noise in Fine Registration of Time-of-Flight Range Data with High-Resolution Surface Data," *Proc. Medical Image Computing and Computer Assisted Intervention*, pp. 251-258, 2010.
- [42] A. Myronenko and X. Song, "Point Set Registration: Coherent Point Drift," *IEEE Trans. Pattern Analysis and Machine Intelligence*, vol. 32, no. 12, pp. 2262-2275, Dec. 2010.



Lena Maier-Hein received the diploma degree (Dipl-Inform) in computer science with distinction from Karlsruhe Institute of Technology (KIT) in 2005. Between 2005 and 2008, she worked on the PhD thesis at the Division of Medical and Biological Informatics at the German Cancer Research Center (DKFZ) and received the PhD (Dr-Ing) degree with distinction in 2009. She received several scholarships and awards, including the Waltraud-Lewenz Prize 2008 for outstanding research at the German Cancer Research Center (DKFZ) and the Ingrid-zu-Solms Prize for Natural Sciences 2009/2010. Her current research interests include the field of computer-assisted medical interventions.



Alfred M. Franz received the diploma degree in medical computer science (Dipl-Inform Med) from the University of Heidelberg in 2012. During his studies, he was involved in many different research projects in the Division of Medical and Biological Informatics at the German Cancer Research Center (DKFZ) Heidelberg, where he is currently working toward the PhD degree. His current research interests include medical image processing, specifically in the area of diagnosis

and treatment support of physicians.



Thiago R. dos Santos received both the BSc and MSc degrees in computer science from the Federal University of Santa Catarina, Florianópolis, Brazil, with distinction. Currently, he is a researcher at the German Cancer Research Center (DKFZ) and working toward the PhD degree at the University of Heidelberg. He was awarded a scholarship for doctoral studies from the German Academic Exchange Service (DAAD) in Germany. His current research

interests include medical image processing and shape modeling, specifically in the areas of surface matching for soft tissue navigation and intra-operative registration.



Mirko Schmidt received the diploma degree in physics from the Friedrich-Schiller University, Jena, Germany, in 2008. From 2008 to 2011, he was a research associate at the Heidelberg Collaboratory for Image Processing (HCI) at the University of Heidelberg. He received the PhD degree in physics from Heidelberg University in 2011. His research project addresses the field of computational photography and 3D Time-of-Flight depth imaging systems, and is sponsored by Sony Deutschland GmbH. He is involved in the definition of the EMVA 1288 Standard for measurements and description of machine vision cameras.



Markus Fangerau is currently studying computer science at the Hochschule Mannheim University of Applied Sciences in Germany. He is working as a research assistant and leads the Medical Embedded Systems Group in the Division of Medical and Biological Informatics of the German Cancer Research Center. His current research interests are mobile medical applications, medical imaging, and visualization. He has extensive experience with compression algorithms, systems programming, procedural models, and distributed systems.



Hans-Peter Meinzer received the MS degree in physics and the BS degree in economics from Karlsruhe University, and received the doctorate in medical computer science from Heidelberg University (formal languages, 1983) and a "habilitation" (cell growth simulation, 1987). He is the director of the Department of Medical and Biological Informatics at the German Cancer Research Center (DKFZ) in Heidelberg and a professor of medical computer science at Heidelberg University. He has won several scientific awards, e.g., from the German Society of Heart Surgery (1992), the German Society of Pattern Recognition (1993), and the European Commission (1997 and 2003), and has won the European Information Technology Prize twice.



J. Michael Fitzpatrick is a professor emeritus of electrical engineering and computer science, of radiology, and of neurosurgery at Vanderbilt University, Nashville, Tennessee, where he has served as a member of the faculty since 1982. His research interests include image guidance for surgery and image registration. He has more than 200 publications and holds 16 patents. He is a fellow of the IEEE and SPIE, coeditor of volume two of the *SPIE Handbook of Medical Imaging*, and served as the cochair of the Image Processing Conference for the SPIE Medical Imaging Symposium for 4 years.

▷ For more information on this or any other computing topic, please visit our Digital Library at www.computer.org/publications/dlib.